

**OPTICAL HAZE PROPERTIES OF POLYETHYLENE BLOWN FILMS:  
PART 2 – THE ORIGINS OF VARIOUS SURFACE ROUGHNESS MECHANISMS<sup>a</sup>**

**Ashish M. Sukhadia**

Group Leader, Polymer Processing  
Chevron Phillips Chemical Company LP  
Bartlesville, OK 74004

**David C. Rohlifing**

Group Leader, Polymer Rheology  
Chevron Phillips Chemical Company LP  
Bartlesville, OK 74004

**Garth L. Wilkes**

University Distinguished Professor  
Department of Chemical Engineering  
Polymer Materials & Interfaces Laboratory  
Virginia Polytechnic Institute & State University  
Blacksburg, VA 24061

**Matthew B. Johnson**

Department of Chemical Engineering  
Polymer Materials & Interfaces Laboratory  
Virginia Polytechnic Institute & State University  
Blacksburg, VA 24061

**ABSTRACT**

In continuation of our associated report here (see Part 1, TAPPI 2001 Conf. Proc.), we have now found that high haze in PE blown films can be caused by very different surface roughness mechanisms having unique origins. The total haze % exhibits a complex parabolic relationship with the logarithm of the recoverable shear strain parameter,  $\gamma_{\infty}$ . At low  $\gamma_{\infty}$ , spherulitic superstructures are formed. As  $\gamma_{\infty}$  increases, an oriented, row-nucleated stacked lamella texture is developed. However, at even higher  $\gamma_{\infty}$ , fine-scale surface roughness due to high melt elastic instabilities is induced. We believe that this is the first time that both very low and very high melt elasticity have been shown as primary causative factors in yielding high haze in PE blown films, albeit for fundamentally very different reasons.

**INTRODUCTION**

Optical properties such as haze and clarity are of considerable importance in the development of polyethylene (PE) blown and cast films for packaging applications. As a result, factors affecting these optical properties have been the focus of investigations for many years [1-13]. It was recognized early on that in PE blown films, haze was caused primarily by the scattering of light due to surface irregularities [1,2,3,10]. These surface irregularities were thought to be a consequence of one of two main mechanisms [2,10] - “extrusion roughness” and “crystallization roughness”. An excellent photographic illustration of the crystallization and extrusion haze phenomena in film-blowing may be found in Figure 2 of reference [12]. Extrusion roughness was attributed to the elastic melt flow effects generated at the exit of the die. Crystallization roughness was postulated to occur due to the formation of crystalline aggregates on or close to the surface of the film.

In our recent publication [14], we investigated the factors affecting the optical properties (haze) of PE blown and cast films with an emphasis on the crystallization roughness phenomenon. Investigation of several blown and cast films made from conventional Ziegler-Natta catalyzed linear-low density PE (LLDPE) as well as metallocene-catalyzed LLDPE (mLLDPE) resins was conducted. We found that the surface roughness in these films was a result of the development of distinct spherulitic-like superstructures formed during the blown or cast film processing. Analysis of the rheological and molecular characteristics of these resins led us to conclude that in PE blown and cast films, the optical haze properties were adversely affected due to enhanced surface roughness, caused by the formation of spherulitic-like superstructures in polymer melts that possessed fast relaxing and low melt elasticity rheological characteristics.

A review of some of the earlier work in this area reveals that both low and high polymer melt elasticity have been shown to be responsible for high haze [2,5-8,10,12]. An improvement (decrease) in blown film haze due to a decrease in the melt elasticity was observed in HP-LDPE resins [5,12]. In contrast, it has also been shown that haze

---

<sup>a</sup> Note: This paper was originally published and presented at the 59<sup>th</sup> Society of Plastics Engineers Annual Technical Conference (ANTEC) held in Dallas, TX, May 6-10 (2001).

decreased with increasing melt elasticity in LLDPE films, either by addition of branched molecules or high molecular weight molecules [13].

We have recently investigated the blown film optical haze behavior of a large number of PE resins and found that haze indeed exhibits a complex relationship with the polymer melt elasticity. In this report, we wish to present these results which we believe will help elucidate the relationship between PE blown film optical haze and polymer rheological properties.

## EXPERIMENTAL

### Melt Rheological Characterization

Small-strain (10%) oscillatory shear measurements were performed on a Rheometrics Scientific, Inc. ARES rheometer using parallel-plate geometry. All rheological tests were performed at 190 °C. The complex viscosity ( $\eta^*$ ) versus frequency ( $\omega$ ) data were then curve fitted using the modified three parameter Carreau-Yasuda (CY) empirical model to obtain the zero shear viscosity –  $\eta_0$ , characteristic viscous relaxation time –  $\tau_\eta$ , and the breadth parameter –  $a$ . Details of the significance and interpretation of the CY model and derived parameters may be found elsewhere [15].

To elucidate the rheological differences among the resins in a more quantitative manner, an estimation of the recoverable shear strain parameter was undertaken. Formally, the recoverable shear strain,  $\gamma_\infty$ , for a rubberlike (Lodge) liquid can be stated to be equal to

$$\gamma_\infty = \frac{N_1}{2\tau} \quad \text{Eqn. (1)}$$

where  $N_1$  is the first normal stress difference and  $\tau$  is the shear stress [16]. At low frequencies, the recoverable shear can be estimated to be equal to

$$\gamma_\infty \sim \frac{G'}{\omega |\eta^*|} \quad \text{Eqn. (2)}$$

where  $G'$  represents the elastic part of the dynamic shear modulus while  $|\eta^*|$  and  $\omega$  represent the magnitudes of the corresponding complex viscosity (using the well known Cox-Merz rule) and frequency, respectively [16]. Applying this approximation in the low frequency range ( $\omega = 0.03 \text{ s}^{-1}$ ) the values for recoverable shear strain parameter were obtained for each resin. The choice of the low frequency at which  $\gamma_\infty$  was estimated rests in the fact that differences in the elastic character of various melts are magnified at low frequencies (or shear rates) since they probe the longest relaxation time behavior at these conditions [8]. Furthermore, the approximation in equation (1) above is only valid at very low frequencies or shear rates [16].

### Melt Index

Melt Index (MI) was measured in accordance with ASTM D-1238, condition F (190°C, 2.16 kg). Density was measured using density gradient columns in accordance with ASTM D-1505.

### Molecular Weight Measurements By Gel Permeation Chromatography (GPC)

Molecular weight distribution (MWD), molecular weight averages ( $M_n$ ,  $M_w$ ,  $M_z$ ) and polydispersity ( $M_w/M_n$ ) were obtained using a Waters 150 CV Plus Gel Permeation Chromatograph using trichlorobenzene as the solvent.

### Blown Film Processing

All the blown film samples were made on a laboratory-scale blown film line using typical linear low-density (LLDPE) conditions as follows: 100 mm (4 inch) die diameter, 1.5 mm (0.060 inch) die gap, 37.5 mm (1.5 inch) diameter single-screw extruder fitted with a barrier screw with a Maddock mixing section at the end (L/D=24, 2.2:1 compression ratio), 115 RPM screw speed [about 27 kg/h (60 lb/h) output rate], 2.5:1 blow up ratio (BUR), “in-pocket” bubble with a “freeze line height” (FLH) between 20-28 cm (8-11 inch), 190 °C (375 °F) barrel and die set temperatures and 1 mil (25 micron) thick film. Cooling was accomplished with a Dual Lip air ring using ambient (laboratory) air at about 25 °C (75-80 °F). These particular processing conditions were chosen since the film properties so obtained are representative of those obtained from larger, commercial scale film blowing conditions.

### Atomic Force Microscopy (AFM)

AFM micrographs were obtained with the use of a Digital Instruments Nanoscope III Scanning Probe Microscope operated in tapping mode. Nanosensor TESP single-beam cantilever tips possessing force constants of  $35 \pm 7$  N/m and oscillated at frequencies of ca. 290 kHz were used.

### Small-Angle Light Scattering (SALS)

The Hv small-angle light scattering patterns were obtained utilizing a He-Ne laser with a wavelength of 632.8 nm. Further details of this technique are described in detail elsewhere [14].

### Haze Measurement

The haze (%) was measured in accordance with the procedures specified in ASTM D 1003-97. The measurements were made on a Haze Gard *Plus*<sup>TM</sup> instrument (Model 4725) made by the BYK-Gardner® Company. To separate the measured total haze into its bulk (or internal haze) and surface (or external haze) components, the following procedure was employed. First, the haze of the as-blown film sample was measured. This is the total haze of the film. Then a very thin layer of a silicone oil [A-Series oil, refractive index ( $n$ ) = 1.512 from Cargille Oil Company] of similar refractive index to that of the film was applied to both sides, i.e. the outside surface of the bubble and the inside surface of the bubble. The haze was measured again. This value is the bulk contribution. Finally, the difference between the total haze value and bulk haze value provided the surface haze contribution directly.

### Materials

A very large number of PE resins, both experimental and commercial, were used to generate the overall trends reported here. These resins were made using metallocene, Ziegler-Natta and chromium oxide type catalysts. Due to the large number of resins employed, it is difficult to provide the details of the molecular, rheological and other properties for every resin. Furthermore, we believe that this data is not needed for every resin in order to understand the overall cause-effect relationships we are trying to present. It is therefore perhaps sufficient to note that the resins fell approximately within this broad range of characteristics viz., density of 0.913 – 0.955 g/cm<sup>3</sup>,  $M_w$  of 70,000 – 250,000 g/mol, and  $M_w/M_n$  of 2.2 – 20. The resins contained none, low or high levels of long chain branching (LCB) depending on the catalyst employed. We include the relevant data for only a few selected resins that are largely representative of the various behaviors we have observed. These resins are shown in Table 1, along with the 25  $\mu$ m blown film haze data. In Table 2, the molecular weight (GPC) data is given along with the rheological data as represented by the Carreau-Yasuda fit parameters discussed earlier.

## RESULTS AND DISCUSSION

We begin by looking at the blown film haze data for nearly 200 different PE resins (as described in the experimental section) as a function of the recoverable shear strain parameter,  $\gamma_{\infty}$ . This data is shown in Figure 1 as a (semi-log) plot of the blown film haze % versus the logarithm of  $\gamma_{\infty}$ . Despite some scatter, the parabolic trend of the data set is evident.

In Figure 2, AFM tilted height images of 25  $\mu$ m blown film surfaces for the resins described in Table 1 are shown. It is worth reiterating here that these particular resin/film samples were chosen since they were representative of the three haze regimes discussed earlier. The AFM data in Figure 2 shows that some type surface asperity or roughness is evident, although of different types and to varying degrees, in all of the samples. These surface asperities, it should be noted, all have overall dimensions that are equal to or higher than the wavelength of visible light viz. 400 – 700 nm (0.4 – 0.7  $\mu$ m) and hence are responsible for the scattering of light that causes haze. Closer inspection of these images reveals several other interesting features. Samples I, F, and A exhibit a “globular” or “rounded” surface topography (as that of a number of balls closely packed together and viewed from the top), with the size of these surface structures decreasing in that order. Sample Z appears to be similar to A in the magnitude of the surface roughness features except that it does not reveal the “rounded” topography. Samples D, J and S exhibit surface topographies that are clearly of a different nature than Samples I, F and A in that their topography is more akin to “ocean waves” or mountainous peaks and valleys, and do not exhibit any of the “globular” nature seen clearly in Sample I.

It of interest here to note that the total, surface and bulk haze data given in Table 1 show conclusively that the vast majority of the total haze, ranging from 63 – 97 % of the total haze, comes from the surface roughness contribution.

Furthermore, it is noteworthy that the total and surface haze contributions of these resins appear to be in the same general order as the degree of surface roughness visually observed in the AFM micrographs in Figure 2.

To address the nature of these different surface topographies, we made use of small-angle light scattering (SALS) which has been well established to be effective in denoting the presence of optically anisotropic superstructures [17,18]. It was observed that blown films I, F and A all showed characteristic evidence of a spherulitic texture or morphology, viz. a four-leaf clover SALS pattern. In contrast, the film samples Z, D, J and S showed no four-leaf clover SALS pattern indicating an absence of any spherulitic texture in these films. Rather, the azimuthally independent Hv SALS patterns observed for samples Z, D, J and S are believed to be a consequence of scattering from rod-like textures or random lamellae, having no organized superstructure [19]. One other useful feature of the Hv SALS patterns is the ability to estimate the average dimensions of the spherulites as detailed in our previous publication [14]. Using this well-established methodology, the average diameter of the spherulites was estimated and is shown in Table 1. The Hv SALS results of the blown films thus indicate a distinct presence of spherulitic texture in samples I, F and A, with the average spherulitic diameter decreasing in that order as well, and an absence of any spherulitic texture for samples Z, D, J and S. We note here that the Hv SALS results for these film samples, and their associated morphologies, were confirmed in the higher magnification AFM height and phase images, which are omitted here for the sake of brevity.

The observed behavior in the three regimes is now explained as follows. The resins in the crystallization haze regime (e.g., samples I and F above) all exhibit relatively low  $\gamma_{\infty}$ . This rheological behavior is expected from melts that have fast melt relaxation characteristics or in other words resins with very short relaxation times. For these types of resins, the polymer melt is able to relax rapidly during the free-surface extensional flow that occurs in the bubble just outside the die. This rapid relaxation results in significant randomization of the melt in this zone. The subsequent nucleation and growth that occurs during crystallization at the FLH occurs then from a melt whose state is closer to being randomly oriented, resulting in the nearly “spherulitic-type” superstructures typically expected from crystallization of a quiescent melt. These superstructures result in enhanced surface roughness and thus high haze [13,14].

In the intermediate haze regime, the resins (e.g., samples A and Z above) possess melt relaxation characteristics that, while still short compared to resins in the extrusion haze regime, exhibit longer relaxation times and higher melt elasticities than resins in the crystallization haze regime. These higher relaxation times inhibit the ability of the melt to relax (or randomize) completely and the melt maintains some degree of molecular orientation that was developed prior to the die exit. The ensuing nucleation and growth crystallization processes for these melts occurs from a partially oriented melt, resulting in the development of either much smaller superstructures (as in sample A), or simply a stacked-lamellar (fibril row-nucleated) type morphology (as in sample Z). Indeed, the fact that a fibril row-nucleated or shish-kebab type texture is developed in blown films from resins of high molecular weight and/or broad MWD has been reported by some of us [20,21] and others [22,23] in the past. The resins in this regime generally exhibit the lowest haze as a result of either very small or no spherulitic-type superstructures being present and the fact that the melt elasticity is not high enough to induce any significant elasticity-driven surface roughness as observed in the extrusion haze regime.

In the extrusion haze regime, the resins (e.g., samples D, J and S above) exhibit considerably different behavior than the resins in both the crystallization and intermediate haze regimes. Specifically, the resins possess high enough melt elasticity that a very fine-scale, elasticity-driven surface roughness is induced as the melt leaves the die. Thus in this regime, a transparent or clear bubble is never observed. It is noteworthy that the high haze developed and observed in this regime occurs well before the polymer melt undergoes crystallization, i.e., well before the FLH. Thus, while some additional surface roughness may develop later due to crystallization effects (which is also of the fibril row-nucleated type), the majority of the haze developed here can be easily attributed to the extrusion/elasticity effects, which are obviously manifested at the die exit itself.

Close inspection of the data in Figure 1 reveals that resins having high haze (40-60 %) are observed in both the crystallization haze regime as well as the extrusion haze regime. Obviously, based on the data above, the high haze in the crystallization regime is due to “spherulitic-like” superstructure, which roughens the surface while high haze in the extrusion haze regime is due to elasticity-driven surface roughness which roughens the surface. To the best of our knowledge, we believe that this is the *first* time it has been recognized and clearly demonstrated that two PE resins may have the same level of total haze as a consequence of two completely different mechanisms or origins.

Furthermore, we believe that this is the first time that both very low and very high melt elasticity have been shown as primary causative factors in yielding high haze in PE blown films, albeit for fundamentally very different reasons. The ramifications of this important recognition rest in the fact that from a molecular design perspective, the solution to improving (lowering) haze in the two regimes is quite the opposite! In the crystallization haze regime, the data in Figure 1 clearly demonstrates that one needs to move towards *higher* melt elasticity to lower haze. In complete contrast, however, in the extrusion haze regime one needs to move towards *lower* melt elasticity to lower haze.

## CONCLUSIONS

It was established in this work, consistent with a large body of prior literature, that surface roughness of the order of the wavelength of visible light ( $0.4 - 0.7 \mu\text{m}$ ) is primarily responsible for high haze in PE blown films, with the internal or bulk contribution to haze being almost negligible. The degree and type of surface roughness developed were found to depend to a large extent, if not primarily, on the rheological properties of the melt. The blown film haze % of a very large number and variety of PE resins was found to exhibit a distinctly parabolic relationship when plotted against the logarithm of the recoverable shear strain parameter,  $\gamma_{\infty}$ , estimated at low frequency ( $0.03 \text{ s}^{-1}$ ). Three distinct regimes of behavior were identified in this parabolic relationship viz., crystallization haze regime, intermediate haze regime and extrusion haze regime. At very low values of  $\gamma_{\infty}$ , in the crystallization haze regime, the resins exhibited high haze due to the development of distinct "spherulitic-like" superstructures, which enhanced surface roughness and hence haze. In this crystallization haze regime, it was shown that haze *decreased* with an *increase* in the melt elasticity. At somewhat higher values of  $\gamma_{\infty}$ , in the intermediate haze regime, the resins generally exhibited the lowest haze values. This was observed to be due to the development of either very small "spherulitic-like" superstructures or none at all, in which case the morphology switched to a fibril row-nucleated type texture. In either case, the degree of surface roughness was diminished, thereby lowering total haze as well. In this intermediate haze regime, the total haze was found to be relatively insensitive to changes in the melt elasticity. At much higher values of  $\gamma_{\infty}$ , in the extrusion haze regime, the resins possessed high melt elasticity, inducing a very fine-scale, elasticity-driven surface roughness that once again increased haze. In this extrusion haze regime, and in complete contrast with the crystallization haze regime, it was shown that haze *decreased* with a *decrease* in melt elasticity. We conclude from the above that both very low and very high melt elasticity characteristics are detrimental to the optical haze properties of PE blown films, albeit for fundamentally very different reasons resulting in very different surface roughness mechanisms. Thus whether an increase or decrease in melt elasticity favors improved (decreased) haze depends on the underlying surface roughness/haze mechanism at work.

## ACKNOWLEDGEMENTS

The authors acknowledge Dr. Jay Janzen and Dr. Rajendra K. Krishnaswamy for several useful discussions. Phillips Petroleum Company is acknowledged for providing all the polyethylene samples used in this study, for partial monetary support and for permission to publish this work.

## REFERENCES

1. Clegg, P. L. and Huck, N. D., "The Effect of Extrusion Variables on the Fundamental Properties of Tubular Polyethylene - Part I", *Plastics*, April, 114 (1961).
2. Huck, N. D. and Clegg, P. L., "The Effect of Extrusion Variables on the Fundamental Properties of Tubular Polythene Film", *SPE Trans.*, July, 121 (1961).
3. Clampitt, B. H., German, D. E., and Hanson, H. D., "Techniques for Measuring Surface and Bulk Optical Properties of Polyethylene Films", *Analytical Chemistry*, 41 (10), 1306 (1969).
4. Williamson, D. A., "Rheology of polyolefins: film grades", *Plast. Polym.*, June, 169 (1970).
5. Fujiki, T., "Concept of Secondary Heterogeneous Structure of Long-Chain Branched Polyethylene", *J. Appl. Polym. Sci.*, 15, 47-66 (1971).
6. Perron, P. J. and Lederman, P. B., "The Effect of Molecular Weight Distribution on Polyethylene Film Properties", *Polym. Eng. Sci.*, 12(5), 340 (1972).

7. Meissner, J., "Basic parameters, melt rheology, processing and end-use properties of three similar low density polyethylene samples", *Pure Appl. Chem.*, 42, 553-612 (1975).
8. Shida, M., Shroff, R. N., and Cancio, L. V., "Correlation of Low Density Polyethylene Rheological Measurements with Optical and Processing Properties", *Polym. Eng. Sci.*, 17(11), 769 (1977).
9. Magill, J. H., Peddada, S. V., and McManus, G. M., "Crystallization-Morphology-Polymer Processing Correlations for IUPAC Low Density Polyethylene", *Polym. Eng. Sci.*, 21(1), 1 (1981).
10. Stehling, F. C., Speed, C. S., and Westerman, L., "Causes of Haze of Low-Density Polyethylene Blown Films", *Macromol.*, 14, 698-708 (1981).
11. Speed, C. S., "Formulating blends of LLDPE and LDPE to design better film", *Plast. Eng.*, (July), 39 (1982).
12. Pucci, M. S. and Shroff, R. N., "Correlation of Blown Film Optical Properties with Resin Properties", *Polym. Eng. Sci.*, 26(8), 569 (1986).
13. Cooke, D. L. and Tikuisis, T., "Addition of Branched Molecules and High Molecular Weight Molecules to Improve Optical Properties of LLDPE Film", *SPE ANTEC Conf. Proc.*, , 22 (1989).
14. Johnson, M. B. *et al.*, "Optical Properties of Blown and Cast Polyethylene Films: Surface versus Bulk Structural Considerations", *J. Appl. Polym. Sci.*, 77, 2845-2864 (2000).
15. Hieber, C. A. and Chiang, H. H., "Some correlations involving the shear viscosity of polystyrene melts", *Rheol. Acta*, 28, 321-332 (1989).
16. Dealy, J. M. and Wissbrun, K. F., "Melt Rheology and Its Role in Plastics Processing", Van Nostrand Reinhold, New York, (1990).
17. Stein, R. S. and Rhodes, M. B., "Photographic Light Scattering by Polyethylene Films", *J. Appl. Phys.*, 31, 1873 (1960).
18. Mohajer, Y., Wilkes, G. L., and Orlor, B., "Effect of Prestrain on the Subsequent Crystallization of a Copolyester of Lactic and Glycolic Acid", *Polym. Eng. Sci.*, 24(5), 319 (1984).
19. Maxfield, J. and Madelkern, L., "Crystallinity, Supermolecular Structure, and Thermodynamic Properties of Linear Polyethylene Fractions", *Macromol.*, 10(5), 1141 (1977).
20. Yu, T. and Wilkes, G. L., "Orientation determination and morphological study of high density polyethylene (HDPE) extruded tubular films: effect of processing variables and molecular weight distribution", *Polym.*, 37, 4675-4687 (1996).
21. Sukhadia, A. M., "The Effects of Molecular Structure, Rheology, Morphology and Orientation on Polyethylene Blown Film Properties", *SPE ANTEC Conf. Proc.*, , 160 (1998).
22. Keller, A. and Machin, M. J., "Oriented Crystallization in Polymers", *J. Macromol. Sci. (Phys.)*, B1(1), 41-91 (1967).
23. Fruitwalla, H. *et al.*, "Characterization of Blown Film Morphology", *J. Plast. Film & Sheeting*, 11, 298 (1995).

**Keywords:** haze, blown films, melt elasticity, LLDPE

**Table 1. Basic resin specifications, 25  $\mu\text{m}$  (1 mil) blown film haze data and spherulite diameter data (from SALS) for a few representative resins from this study.**

Resin	I	F	A	Z	D	J	S
Melt Index (dg/min)	2.6	1.2	1.0	1.0	0.2	0.3	0.3
Density (g/cm <sup>3</sup> )	0.919	0.918	0.918	0.921	0.923	0.922	0.917
Haze regime <sup>a</sup>	cryst.	cryst.	int.	int.	ext.	ext.	ext.
Total Haze, H,t (%)	27.5	14.9	2.5	8.6	49.4	62.8	93.1
Bulk Haze, H,b (%)	1.4	1.9	0.9	1.3	2.4	2.8	2.9
Surface Haze, H,s (%)	26.1	13.0	1.6	7.3	47.0	60.0	90.2
H,s/H,t * 100 (%)	94	87	63	85	96	96	97
Spherulite diameter from SALS ( $\mu\text{m}$ )	3.3	2.3 <sup>b</sup>	1.7 <sup>b</sup>	None <sup>c</sup>	None <sup>c</sup>	None <sup>c</sup>	None <sup>c</sup>

<sup>a</sup> cryst. – Crystallization; int. – Intermediate; ext. – Extrusion; See text for details

<sup>b</sup> Rough estimate only since this SALS pattern did not exhibit a definitive maximum in the scattered intensity

<sup>c</sup> Hv SALS did not exhibit any discrete “four-leaf-clover” pattern, indicating an absence of spherulitic superstructure.

**Table 2. Molecular weight and rheology data for a few representative resins from this study.**

Resin	I	F	A	Z	D	J	S
$M_n$ (kg/mol)	33.15	44.76	42.53	23.21	11.47	21.96	11.06
$M_w$ (kg/mol)	70.23	103.07	100.95	115.53	193.62	163.20	107.42
$M_z$ (kg/mol)	134.2	207.5	199.17	494.56	2079.4	1268.3	497
$M_w/M_n$	2.1	2.3	2.4	5.0	16.9	7.43	9.7
$\eta_0$ (Pa.s)	2.81E+3	5.69E+3	6.57E+3	1.69E+4	4.75E+5	1.25E+5	9.77E+4
$\tau_\eta$ (s)	7.61E-3	12.2E-3	1.06E-2	3.13E-2	1.35	0.38	0.55
$a$	0.784	0.734	0.597	0.370	0.187	0.226	0.198
Recoverable Shear Strain x 1E3	1.8	3.3	10	91	443	337	384

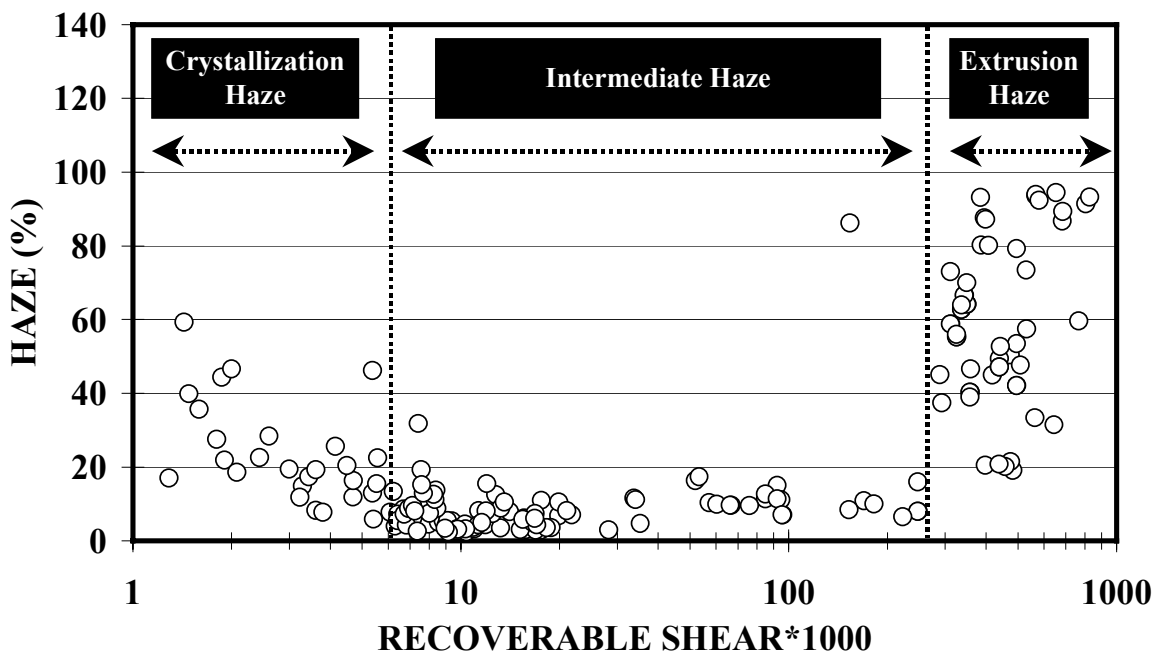


Figure 1. The effect of polymer melt elasticity as represented by the recoverable shear strain parameter on the optical haze of 25  $\mu\text{m}$  (1 mil) blown films. Nearly 200 data points are represented in this plot.

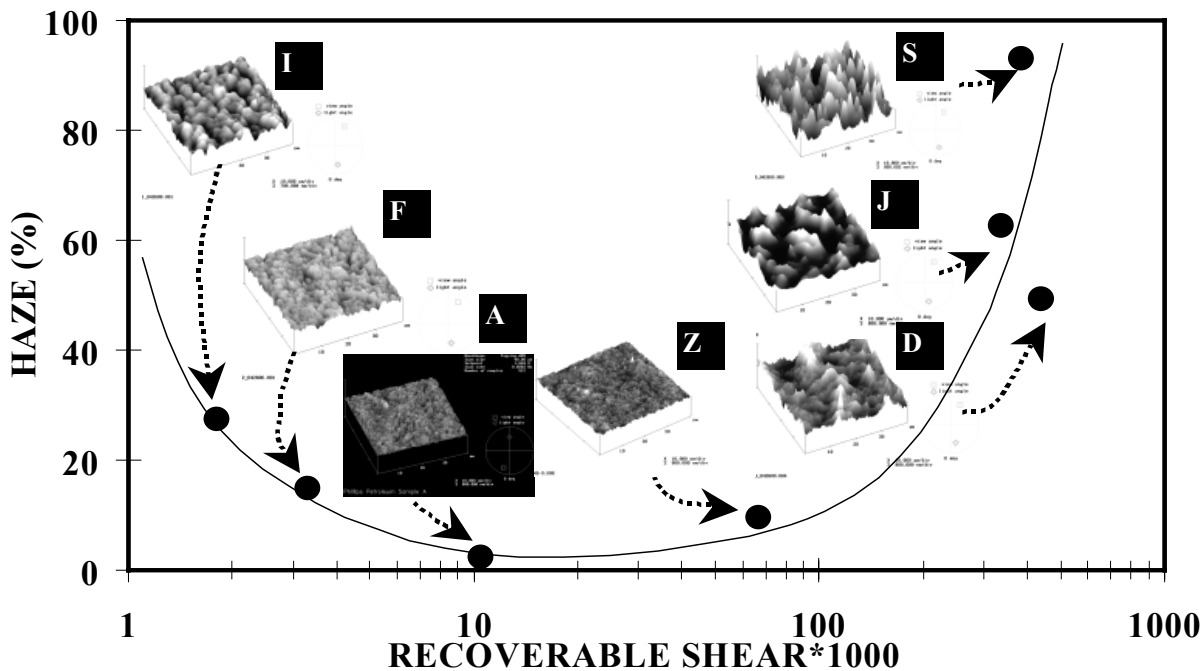


Figure 2. AFM tilted height images 25 micron (1 mil) blown film surfaces. Solid circles in this figure are actual data points, solid line is a trendline. Nomenclature follows Table 1. All images are to the same scale viz. 1600 nm (vertical) x 40  $\mu\text{m}$  x 40  $\mu\text{m}$ .